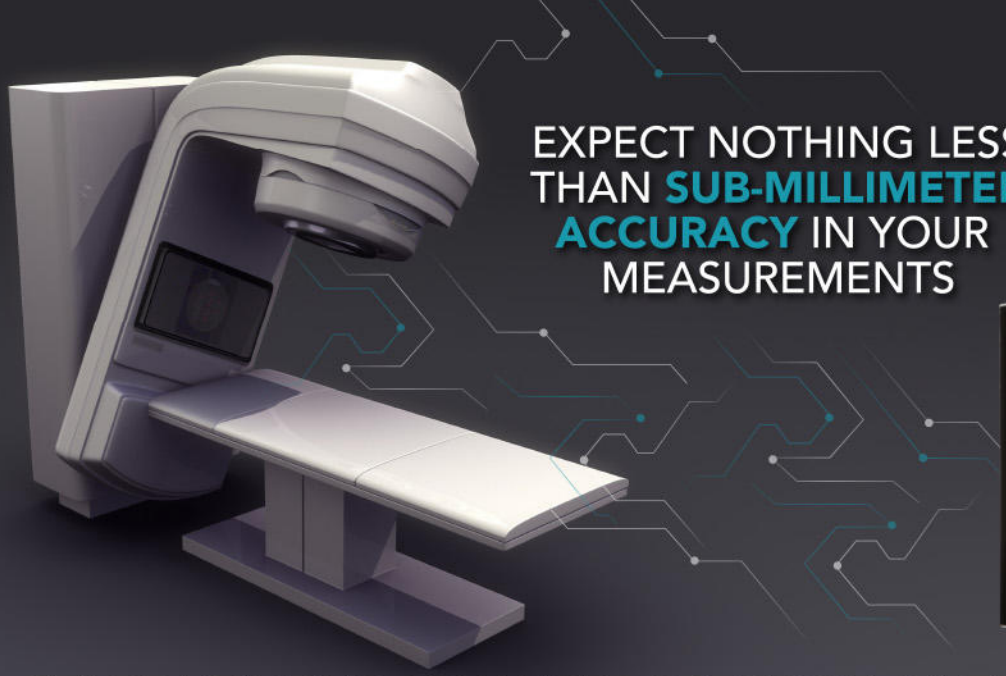

EXPECT NOTHING LESS THAN SUB-MILLIMETER ACCURACY IN YOUR MEASUREMENTS

RIT®

START UTILIZING ADVANCED PRECISION QA TODAY

THE RIT FAMILY OF PRODUCTS **VERSION 6.7.X**

3D Winston-Lutz Isocenter Optimization
The enhanced isocenter optimization routine allows for optimal cone detection, resulting in the utmost precision. The accuracy of this routine now surpasses sub-millimeter resolution. *(Pictured above)*

Cerberus 2.0: The Future of Complete Automation
Completely streamline your automated phantom analysis workflow with the new Cerberus. Cerberus operates in the background of your workstation, allowing for hands-free Imaging QA.

One-Click, Instant Automated Phantom Analyses

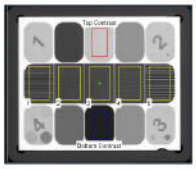

RIT's full suite of phantom analyses provides fast, robust, and accurate analysis of all imaging tests recommended in TG-142. The software now offers added support for the QCkV-1 phantom. *(Pictured right)*

Tolerance Customization and Management
RIT's new Tolerance Manager offers comprehensive customization of tolerance values for every measurement used in all automated phantom analyses. Tolerance profiles can be precisely-tailored to each individual machine in use.

CLICK HERE TO DOWNLOAD TODAY

Elekta Leaf Speed Analysis
RIT now offers fast and accurate automated analysis for Elekta MLC QA. The new Leaf Speed Analysis routine measures the consistency and accuracy of the MLC leaf speeds as they traverse the imager.

TomoTherapy® Registration for Patient QA
Easily perform exact dose comparisons with RIT's new TomoTherapy Registration routine. This new, innovative wizard uses a TomoTherapy® plan, dose map, and a film to determine position an dose accuracy using the red lasers. *(Pictured below)*

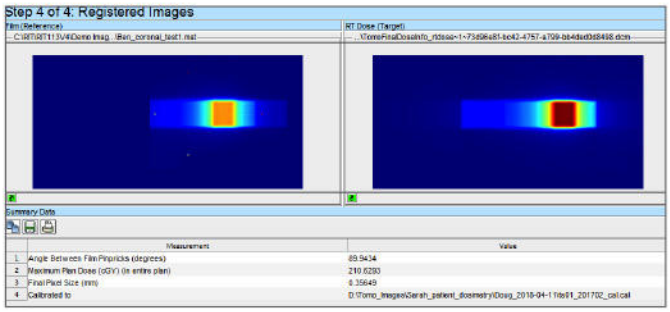

Streamline Your QA Workflow
Fully-customize your software experience with RIT's updated and dynamic interface. With the new ability to hide/display any features or sections, you can instantly access you most frequently-performed analysis routines.

Convenient, Cloud-Based Software Licensing
Easily manage your software licenses with RIT's new, flexible system at your convenience, 24/7/365 without the help of RIT Technical Support. Upgrading is now easier than ever.

RADIOLOGICAL IMAGING TECHNOLOGY, INC.
RADIMAGE.COM
(+1) 719.590.1077 x211 // sales@radimage.com

Connect with RIT
@RIT4QA

Radioembolization lung shunt estimation based on a ^{90}Y pretreatment procedure: A phantom study

Britt Kunnen[a)], Sandra van der Velden, and Remco Bastiaannet
Radiology and Nuclear Medicine, UMC Utrecht, P.O. Box 85500, 3508 GA Utrecht, The Netherlands
Image Sciences Institute, UMC Utrecht, University Utrecht, Heidelberglaan 100, 3584 CX Utrecht, The Netherlands

Marnix G. E. H. Lam
Radiology and Nuclear Medicine, UMC Utrecht, P.O. Box 85500, 3508 GA Utrecht, The Netherlands

Max A. Viergever
Image Sciences Institute, UMC Utrecht, University Utrecht, Heidelberglaan 100, 3584 CX Utrecht, The Netherlands

Hugo W. A. M. de Jong
Radiology and Nuclear Medicine, UMC Utrecht, P.O. Box 85500, 3508 GA Utrecht, The Netherlands

(Received 29 May 2018; revised 20 August 2018; accepted for publication 28 August 2018; published 21 September 2018)

Purpose: Prior to ^{90}Y radioembolization, a pretreatment procedure is performed, in which ^{99m}Tc-macroaggerated albumin (^{99m}Tc-MAA) is administered to estimate the amount of activity shunting to the lungs. A high lung shunt fraction (LSF) may impose lower prescribed treatment activity or even impede treatment. Accurate LSF measurement is therefore important, but is hampered by the use of MAA particles, which differ from ^{90}Y microspheres. Ideally, ^{90}Y microspheres would also be used for the pretreatment procedure, but this would require the activity to be lower than an estimated safety threshold of about 100 MBq to avoid unintended radiation damage. However, ^{90}Y is very challenging to image, especially at low activities (<100 MBq). The purpose of this study was to evaluate the performance of three nuclear imaging techniques in estimating the LSF in a low activity ^{90}Y pretreatment scan, using an anthropomorphic phantom: (a) positron emission tomography/computed tomography (PET/CT), (b) Bremsstrahlung single photon emission tomography/computed tomography (SPECT/CT), and (c) planar imaging.
Methods: The lungs and liver of an anthropomorphic phantom were filled with ^{90}Y chloride to acquire an LSF of 15%. Several PET/CT (Siemens Biograph mCT), Bremsstrahlung SPECT/CT (Siemens Symbia T16) and planar images (Siemens Symbia T16) were acquired at a range of ^{90}Y activities (1586 MBq down to 25 MBq). PET images were reconstructed using a clinical protocol (attenuation correction, TOF, scatter and random correction, OP-OSEM), SPECT images were reconstructed using both a clinical protocol (attenuation correction, OSEM) and a Monte Carlo (MC)-based reconstruction method (MC-based detector, scatter, and attenuation modeling, OSEM), for planar images the geometric mean was calculated. In addition, in all cases except clinical SPECT, background correction was included. The LSF was calculated by assessing the reconstructed activity in the lungs and in the liver, as delineated on the CT images. In addition to the 15% LSF, an extra "cold" region was included to simulate an LSF of 0%.
Results: PET reconstructions accurately estimated the LSF (absolute difference <2 percent point (pp)) when total activity was over 200 MBq, but greatly overestimated the LSF (up to 25pp) when activity decreased. Bremsstrahlung SPECT clinical reconstructions overestimated the LSF (up to 13pp) when activity was both high and low. Similarly, planar images overestimated the LSF (up to 23pp). MC-based SPECT reconstructions accurately estimated the LSF with an absolute difference of less than 1.3pp for activities as low as 70 MBq.
Conclusions: Bremsstrahlung SPECT/CT can accurately estimate the LSF for a ^{90}Y pretreatment procedure using a theoretically safe ^{90}Y activity as low as 70 MBq, when reconstructed with an MC-based model. [https://doi.org/10.1002/mp.13168]

Key words: lung shunt fraction, PET, radioembolization, SPECT, yttrium-90 pretreatment procedure

1. INTRODUCTION

Radioembolization is an established treatment for unresectable liver tumors where ^{90}Y-loaded microspheres are administered in the arterial vasculature of the liver. Before the treatment dosage is administered, a dosage of ^{99m}Tc-macroaggerated albumin (^{99m}Tc-MAA) is administered to simulate ^{90}Y microsphere distribution.[1] We will refer to this

procedure as the pretreatment procedure. A single photon emission tomography/computed tomography (SPECT/CT) of the ^{99m}Tc-MAA is acquired to detect potential extrahepatic depositions, and the lung shunt fraction (LSF) is estimated based on planar scintigraphy. However, the accuracy of this LSF estimation is uncertain and may be improved by using SPECT/CT images instead of planar scintigraphy.[1–4] Other problems regarding the accuracy of the LSF estimation still remain. First, the LSF may be overestimated by the MAA particles because of free circulating pertechnetate.[5] Second, the accuracy and reproducibility of the LSF estimation is thought to be affected by differences in shape and size distribution between MAA particles and microspheres.[6,7] These problems could be solved by using a particle for the pretreatment procedure that is identical to the particle used for treatment, as is the essence of the ^{166}Ho microsphere treatment approach.[8]

We have investigated the possibility of using ^{90}Y microspheres for the pretreatment procedure to improve the estimation of the LSF for ^{90}Y radioembolization. However, since ^{90}Y is an almost pure beta-emitter, it raises some concerns with regard to the safety of using it for the pretreatment procedure. Low activities are preferred to avoid unintended radiation damage. For ^{166}Ho radioembolization, a pretreatment procedure using an activity of 250 MBq, which is imaged by planar scintigraphy and SPECT/CT, is currently used in clinical studies and has been shown safe.[8–11] The total energy absorbed from the decay of 1 MBq of ^{166}Ho is 15.9 mJ, whereas the total energy absorbed from the decay of 1 MBq of ^{90}Y is 49.4 mJ.[9,12] Because the energy deposition of ^{90}Y is 3.11 times higher than that of ^{166}Ho, theoretically a lower activity for ^{90}Y pretreatment procedures should be used to be as safe as the current clinical ^{166}Ho protocol, for example an activity around 80–100 MBq. This low activity (<100 MBq) imposes some difficulties for imaging.

^{90}Y imaging with positron emission tomography (PET) is based on the small decay branch of ^{90}Y generating positrons. Only 32 in a million decays result in positron emission.[13] This small positron decay ratio is sufficient for posttreatment dosimetry when patients receive a high amount of activity (treatment), but it may not be sufficient to accurately estimate the LSF when the activity is strongly reduced (pretreatment procedure).[2] ^{90}Y PET accuracy under low count conditions has been investigated with phantom studies.[7,14–17] These studies focused on lesion detectability, recovery coefficients, reconstruction algorithms, and image acquisition parameters. However, to estimate the LSF, one must quantify very low activity concentrations. Activity recovery of a low concentration (37 kBq/mL) of ^{90}Y has been described by Willowson et al.[14] However, for a pretreatment procedure one needs to be able to measure even lower activity concentrations, especially in the lung area (<10 kBq/mL, based on an activity of 100 MBq, maximum LSF of 20% and a lung volume of 2 L).

Another possibility for ^{90}Y imaging is SPECT based on Bremsstrahlung photons. Bremsstrahlung photons have a very broad and continuous spectrum which prohibits the use of scatter windows for scatter correction. Scatter correction for Bremsstrahlung SPECT therefore relies on time-consuming Monte Carlo (MC) reconstruction models. Although there is general consensus that ^{90}Y PET produces superior image quality over Bremsstrahlung SPECT,[18] Bremsstrahlung SPECT is more sensitive than ^{90}Y PET and might therefore be better suited to estimate low activities.

In this study, an anthropomorphic phantom was used to investigate whether the LSF of a ^{90}Y pretreatment procedure can be accurately determined by ^{90}Y PET/CT, Bremsstrahlung SPECT/CT, and/or planar scintigraphy.

2. MATERIALS AND METHODS

2.A. Phantom

We used an anthropomorphic thorax phantom (Radiology Support Devices, Long Beach, CA), which represents the torso of an average male (Fig. 1). The phantom was designed to realistically simulate PET and SPECT acquisitions. It includes the bone structures within the torso and fillable compartments representing the liver and lungs.

The liver (1.1 L) was filled with an initial activity of 1347 MBq, as measured by a dose calibrator (VDC-404, Veenstra Instruments), of ^{90}Y chloride in 0.5 M of HCl to prevent adhesion to the plastic phantom walls.[19] The lungs, filled with styrofoam beads, were filled with a total initial activity of 239 MBq of ^{90}Y chloride in 0.5 M of HCl. The total volume of the lungs was 2.0 L and their density was 0.40 g/cm^3. The remainder of the thorax phantom was filled with water. The total initial activity of the phantom, 1586 MBq, was comparable to a clinically used treatment dosage of ^{90}Y resin microspheres (SIR-Spheres®, Sirtex, Sydney, Australia).[20,21] The phantom was imaged multiple times during decay, down to a final total activity of 25 MBq,

FIG. 1. Anthropomorphic thorax phantom with lung and liver inserts. [Color figure can be viewed at wileyonlinelibrary.com]

which is well below the estimated safety threshold of about 100 MBq for a ^{90}Y pretreatment procedure.

The LSF was defined as the activity in the lungs divided by the activity in the lungs and the liver.[1] Resin microspheres are contraindicated in patients who have an LSF of more than 20%. It is advocated to reduce the prescribed activity in patients who have an LSF between 10% and 20%.[22] Glass microspheres (TheraSphere®, BTG, London, UK) are contraindicated in patients whose LSF could result in a delivery of more than 610 MBq of ^{90}Y to the lungs (i.e., approximately 30 Gy for 1 kg lungs).[23] The LSF of our phantom was 15%. This LSF was chosen because it is within the range where LSF-indicated activity reductions are generally advocated; therefore, the LSF needs to be accurately estimated within this range.

2.B. Image acquisition

Twelve PET/CT scans, twelve SPECT/CT scans, and twelve planar scintigraphy images were acquired over a period of six half-lives to include a broad range of ^{90}Y activities ($t_{1/2}$ = 64.1 h, Table I).

PET/CT images were acquired on a Siemens Biograph mCT time-of-flight (TOF) system. Three bed positions were scanned to fit the entire phantom in the field of view (FOV). Acquisition time was 15 min per bed position (in agreement with our clinical protocol[24]) (total acquisition time of 45 min) and consecutive bed positions overlapped approximately 43%. A CT scan (120 kVp, 39 mAs) was made for attenuation correction and to support organ delineation.

SPECT/CT and planar images were acquired on a dual head Siemens Symbia T16 system. For the SPECT/CT scans, the lungs and liver of the phantom fit in a single FOV. Data were acquired in a 50–250 keV energy window with the high-energy collimators mounted.[25] Projections were acquired for 30 s per angle, using 120 angles over 360° (total acquisition time of 30 min). These acquisition parameters were identical to our clinical settings.[24] A CT scan (110 kVp, 30 mAs) was made for attenuation correction and to support organ delineation.

Planar scintigraphy images were acquired by means of a whole body scan with a scanning speed of 5 cm/min (total acquisition time of 20 min). The two gamma cameras were positioned opposite each other to acquire anterior and posterior images. Data were acquired in a 50–250 keV energy window with the high-energy collimators mounted.

For both SPECT and planar acquisitions, a single background measurement was performed without the phantom present using the settings described above. For PET, a single long background measurement (total scan time of 24 h) was performed with the phantom without activity in the scanner.

2.C. Image reconstruction

For each imaging modality, data were reconstructed using the clinical protocol of our institution. In addition, a background correction was performed for each modality.

For PET data, the first reconstruction method (PET-clinical) was a clinically used reconstruction algorithm on the scanner console. This is an ordinary Poisson ordered subset expectation maximization (OP-OSEM) reconstruction method, including resolution recovery (TrueX), TOF information, random, attenuation, scatter, dead time, and decay correction. Random correction was based on smoothed delayed coincidences. Attenuation correction was based on a CT scan. Images were reconstructed using four iterations with 21 subsets and a 5 mm full width at half maximum (FWHM) Gaussian postreconstruction filter was applied. The reconstructed voxel size was 4.1 × 4.1 × 3.0 mm^3. Because ^{90}Y is not provided on the isotope list of the scanner, ^{89}Zr was used as an alternative isotope for acquisition and reconstructed images were corrected for the different half-life and positron branching ratio. The second method (PET-BGcorr) included a background correction in which the activity in the volumes of interest (VOIs) of the background image (reconstructed as described above) was subtracted from the activity in the VOIs of the phantom image.

For SPECT data, the first reconstruction method (SPECT-clinical) was a clinically used two-dimensional OSEM (2D OSEM) algorithm using eight iterations with five subsets. Attenuation correction was based on a CT scan. No scatter correction or postreconstruction filter was applied. The reconstructed voxel size was 2.4 × 2.4 × 2.4 mm^3. The second algorithm (SPECT-MC) was an MC-based OSEM algorithm. In this reconstruction method scatter, attenuation, and collimator-detector response were MC simulated. This reconstruction method and its validation are described in detail by Elschot et al.[26] Since MC-based reconstructions take longer to converge, images were reconstructed using 60 iterations and eight subsets.[26] No postreconstruction filter was applied. The reconstructed voxel size was 4.8 × 4.8 × 4.8 mm^3. The third algorithm (SPECT-MC-BGcorr) was the same as the SPECT-MC algorithm, but in addition included a background correction in this MC reconstruction algorithm by adding the average measured background count to each forward projection.

Planar images were created from the geometric means of the anterior and posterior images and the pixel size was

TABLE I. Phantom activities at time of acquisition.

Scan number	1	2	3	4	5	6	7	8	9	10	11	12
Total phantom activity at PET acquisition (MBq)	1570	946	557	336	220	100	89	70	54	42	35	25
Total phantom activity at SPECT acquisition (MBq)	1550	959	565	341	223	119	88	70	55	42	35	26
Total phantom activity at planar scintigraphy (MBq)	1524	952	561	338	221	118	87	69	54	42	35	26

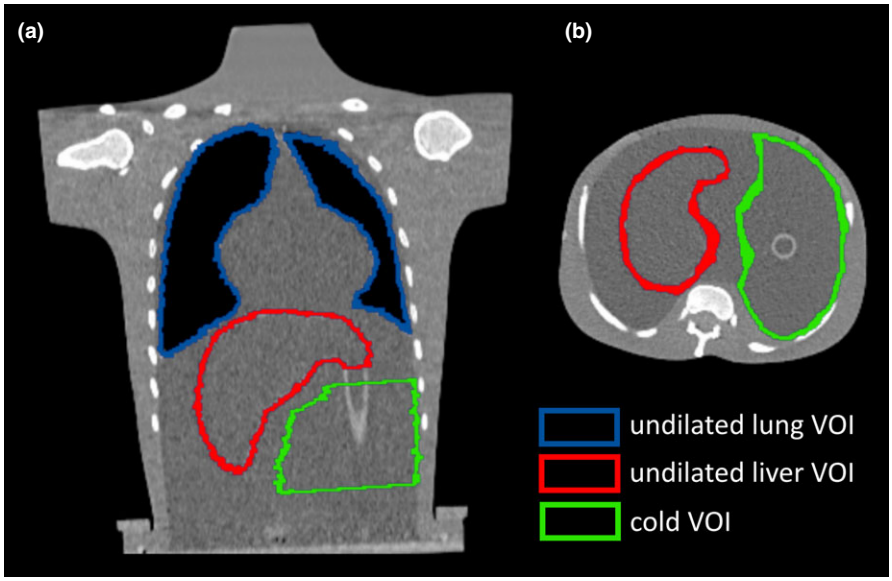

FIG. 2. Coronal (a) and axial (b) views of a CT of the anthropomorphic thorax phantom. [Color figure can be viewed at wileyonlinelibrary.com]

2.4×2.4 mm^2 (planar-clinical). Background correction was performed by subtracting the counts in the regions of interest (ROIs) of the background image from the counts in the ROIs of the phantom image (planar-BGcorr).

2.D. Analysis

The lungs and the liver were manually delineated on one CT scan to create a lung and a liver volume of interest (VOI). This reference CT was rigidly registered to all other CT scans and the VOI of the liver was transformed accordingly to ensure that the same volume was analyzed for each scan. In between scans, during transport, the lungs could slightly move within the phantom which could induce slight differences in position for each scan. Therefore, for each lung, a separate rigid registration from the reference CT to all other CTs was performed. VOIs of the lungs were transformed accordingly. All registrations and transformations were performed using Elastix and visually inspected.[27]

To partly compensate for partial volume effects, the VOIs were dilated by the spatial resolution of each system, 6 mm for PET and 14 mm for SPECT. When this dilation resulted in overlapping VOIs, the liver VOI had priority over the lung VOI. This approach was equal to what is used in clinical LSF analysis. VOIs were transferred to the PET and SPECT reconstructions and the LSF was calculated by dividing the activity in the lung VOI by the activity in the lung and liver VOIs. The recovery coefficient was calculated by dividing the observed activity by the true activity. Because SPECT and planar images hold counts instead of Bq/mL like PET, the observed activity for these modalities is based on the known total activity in the phantom as:

$$A_{ROI} = \frac{A_{tot}}{C_{lung} + C_{liver}} C_{ROI},$$

where A_{ROI} is the observed activity in either the lung or liver ROI, A_{tot} is the total activity of the phantom at the time of imaging, C_{lung} is the amount of lung counts, C_{liver} is the amount of liver counts and C_{ROI} is the amount of counts in either the lung of the liver ROI.

The LSF of the anthropomorphic phantom in this study was 15%. However, the majority of radioembolization patients have an LSF < 10%.[20] These patients should be identified as suitable for treatment without the need of dosage reduction. To examine the accuracy of the LSF estimations for low LSFs, an extra region, apart from the lungs and the liver, was delineated on the reference CT. This region was a large (1.5 L), fully connected VOI located below the liver that fitted inside the FOV of all scans (Fig. 2). It held cold (no activity present) water and served to simulate lungs with no activity (LSF of 0%). This cold VOI was transformed to the other CT scans according to the liver transformations previously described. The cold VOI had a smaller volume than the lung VOI, which leads to a smaller LSF estimate for equal activity concentrations. To compensate for this volume difference, the activity in the cold VOI was scaled to the lung volume by multiplying the activity in the cold VOI by the fraction of lung VOI volume over cold VOI volume.

For planar images, all previously described 3D VOIs from the corresponding SPECT/CT scans were projected to form 2D ROIs. Since the planar images had no reference to the CT scans, the liver ROI was manually positioned over the hot liver region in the planar image, which was clearly visible on all images. This approach was equal to what is used in clinical LSF analysis. The same transformation was then applied to the lung and cold ROIs, because the phantom was not moved between the SPECT/CT and the planar acquisition. The LSF was calculated as described previously.

In order to get an estimate of the error margins on these LSF measurements, we varied the dilation applied to the lung

TABLE II. Number of counts/true coincidences acquired.

	Scan 1 (~1550 MBq)	Scan 12 (~26 MBq)	Background measurement (0 MBq)
Counts acquired during SPECT exam (30 min)	1.9×10^7	6.0×10^5	2.8×10^5
Counts acquired during planar imaging (20 min)	6.1×10^6	2.3×10^5	1.3×10^5
True coincidences acquired during PET exam (45 min)	3.9×10^5	1.7×10^4	3.0×10^5 (24-h exam) 9.3×10^3 (scaled to 45-min exam)

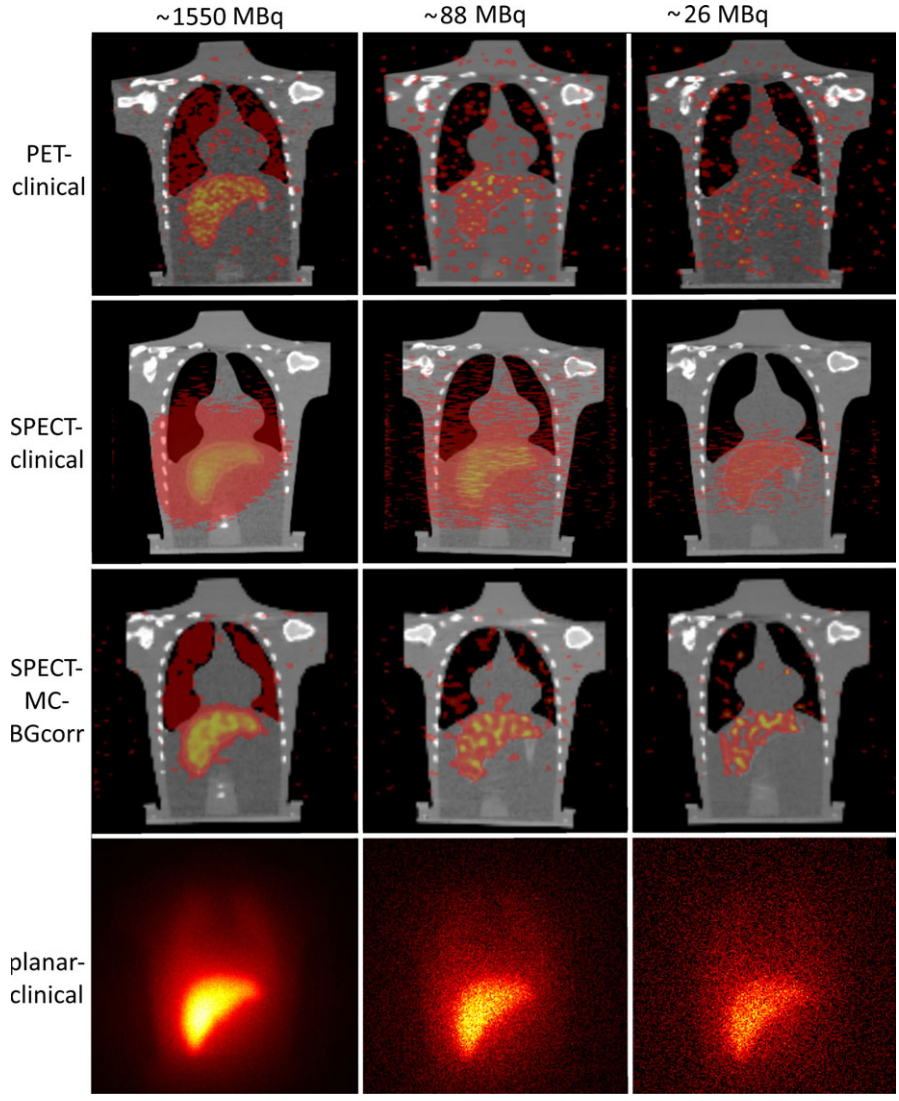

FIG. 3. Coronal views of the PET-clinical, SPECT-clinical, and SPECT-MC-BGcorr reconstructions and geometric means of the planar-clinical images for scans with a total phantom activity of approximately 1550, 88 and 26 MBq. [Color figure can be viewed at wileyonlinelibrary.com]

and liver VOIs by ±5 mm. This represented the variation in delineation caused by different observers.

3. RESULTS

The number of counts or true coincidences acquired during the different exams is listed in Table II.

Figure 3 shows the coronal views of the PET and SPECT reconstructions and the planar images for scans with a total phantom activity of approximately 1550, 88 and 26 MBq. For total activities over ~350 MBq, the PET reconstructions had a visually higher spatial resolution than the SPECT reconstructions. For total activities below ~350 MBq, the PET reconstructions were more noisy and below ~70 MBq the liver was no longer identifiable.

SPECT-clinical reconstructed a hot liver for all scans, but with substantial spillover activity outside the liver. Part of this spillover activity was reconstructed inside the lungs, but there

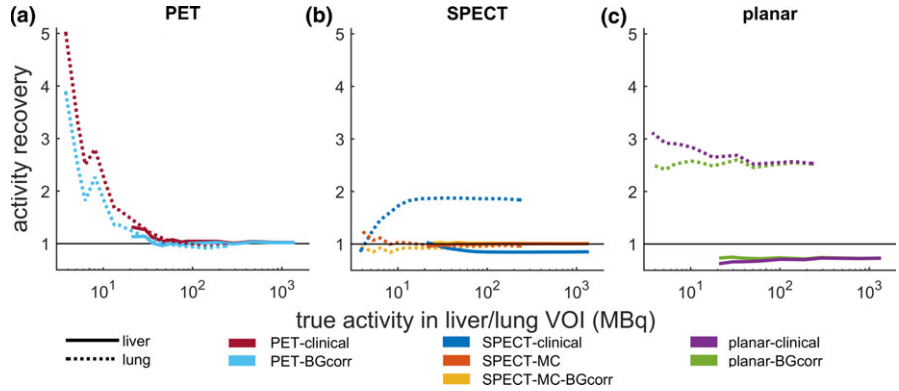

FIG. 4. Activity recovery for the liver (solid lines) and the lungs (dotted lines), for PET (a), SPECT (b), and planar images (c). Recovery coefficients >1 indicate overestimation of true activity, recovery coefficient <1 indicate underestimation of true activity. [Color figure can be viewed at wileyonlinelibrary.com]

was no visual homogeneous activity reconstructed inside the lungs (the upper parts of the lungs had no reconstructed activity in any of the scans).

SPECT-MC and SPECT-MC-BGcorr were visually very similar (SPECT-MC had slightly more noise than SPECT-MC-BGcorr). Both reconstructed uniform activity in both the liver and the lungs for total activities over ~500 MBq. For total activities below ~500 MBq, the reconstructions were more noisy, but in contrast to PET, the liver was still visible in all reconstructions.

Planar images showed the liver clearly, just like the SPECT-clinical reconstructions, but with substantial (scattered) background and spillover activity.

Figure 4 shows the activity recovery of the liver and the lungs for all imaging modalities. For PET, activity recovery was accurate (less than 10% difference) for activities over 45 MBq, but activity was largely overestimated for activities below 35 MBq. This overestimation was slightly reduced by performing a background correction.

SPECT-clinical shows overestimation of activity in the lungs and underestimation of activity in the liver. The SPECT-MC reconstruction method shows large improvement over the SPECT-clinical reconstruction method. Using an MC-based reconstruction method led to accurate activity recovery (less than 10% difference) for activities over 10 MBq. Including a background correction in the MC-based reconstruction method had most effect on the scans with a total activity below 100 MBq. The activity recovery of the SPECT-MC-BGcorr varies between 1.01 and 1.03 for the liver compartment and between 0.84 and 0.97 for the lung compartment. The activity recovery of the SPECT-MC varies between 0.95 and 1.01 for the liver compartment and between 0.96 and 1.26 for the lung compartment.

Planar images largely overestimated the activity in the lungs and underestimated the activity in the liver, for the full range of activities. The background correction made the activity recovery more stable over the range of activities, but did not completely correct for the over- and underestimation in the lungs and liver, respectively.

Figures 5(a), 5(b), 5(c) show the estimated LSF for a true LSF of 15%. PET accurately estimated the LSF (absolute difference <2 percent point (pp)) for total activities over 200 MBq (absolute difference of 0.6pp (PET-clinical) and 0.8pp (PET-BGcorr) at 1570 MBq), but started to overestimate (up to 25pp) the LSF as the activity decreased. The background correction had most effect on scans with a total activity below 100 MBq. Furthermore, the LSF was more sensitive to varying delineations as the activity decreased, shown by the increasing shaded area.

SPECT-clinical overestimated the LSF for almost all activities (absolute difference of 13pp at 1550 MBq), as expected based on visual inspections of the reconstructions. Similarly, planar imaging largely overestimated the LSF for all scans (absolute difference between 21pp and 31pp).

SPECT-MC and SPECT-MC-BGcorr both estimated the LSF accurately for total activities over 70 MBq (absolute difference of 0.5pp (SPECT-MC) and 0.6pp (SPECT-MC-BGcorr) at 1550 MBq and an absolute difference of 0.5pp (SPECT-MC) and 1.3pp (SPECT-MC-BGcorr) at 70 MBq). Furthermore, the uncertainty represented by the shaded area was quite small for total activities over 70 MBq (±0.9pp (SPECT-MC) and ±0.5pp (SPECT-MC-BGcorr) at 70 MBq).

Figures 5(d), 5(e), 5(f) show the LSF based on the cold VOI, simulating an LSF of 0%. PET estimated the LSF accurately only for the scan with a total activity of 1570 MBq (absolute difference of 1.7pp (PET-clinical) and 1.3pp (PET-BGcorr)), but largely overestimated the LSF as the activity decreased (up to 35pp).

Planar-clinical, planar-BGcorr and SPECT-clinical overestimated the LSF, similarly to the overestimation seen for the LSF of 15%.

SPECT-MC and SPECT-MC-BGcorr estimated the LSF accurately for total activities over 100 MBq (absolute difference of 1.0pp (SPECT-MC) and 0.8pp (SPECT-MC-BGcorr) at 1550 MBq). As the activity decreased, SPECT-MC-BGcorr outperformed SPECT-MC, having a more accurate LSF estimation (absolute difference of 2.4pp (SPECT-MC-BGcorr) vs 4.6pp (SPECT-MC) at 70 MBq) and less uncertainty in its LSF estimation (±0.5pp (SPECT-MC-BGcorr) vs ±0.8pp (SPECT-MC) at 70 MBq).

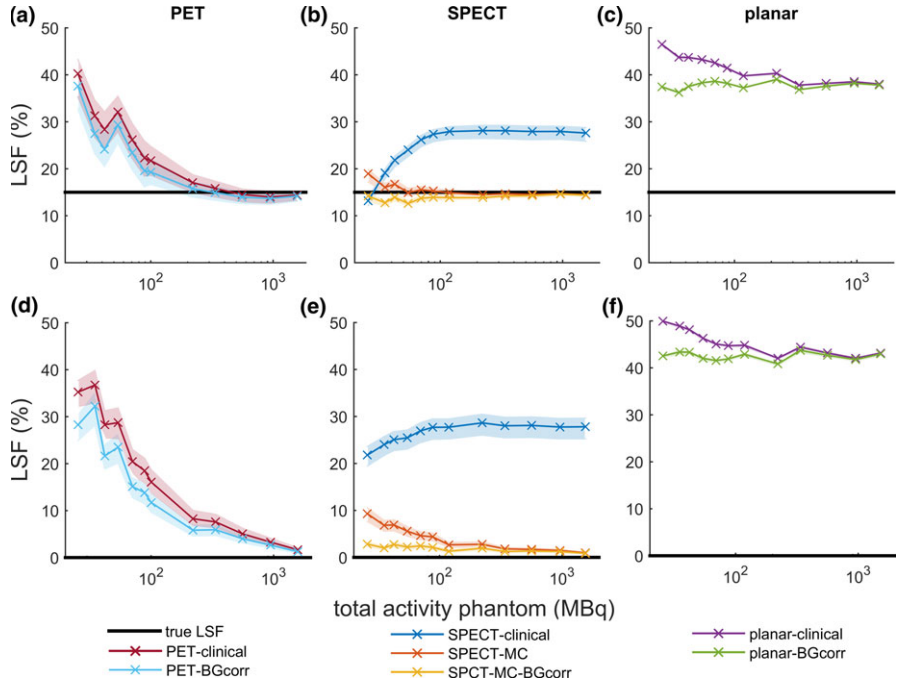

FIG. 5. LSF for PET (a, d), SPECT (b, e), and planar images (c, f) as a function of total ^{90}Y activity in the phantom. The horizontal black lines indicate the true LSF of the phantom, which is either 15% (a, b, c) or 0% (d, e, f). Shaded areas show the uncertainty in the LSF caused by varying the dilation of the VOIs by ±5 mm. [Color figure can be viewed at wileyonlinelibrary.com]

4. DISCUSSION

This study evaluated the ability to accurately estimate the LSF of ^{90}Y-based radioembolization by means of a low activity ^{90}Y-based pretreatment procedure. The imaging methods investigated comprised PET/CT, Bremsstrahlung SPECT/CT and planar imaging. We found that Bremsstrahlung SPECT/CT, when reconstructed with an MC-based model including a background correction, estimated the LSF down to activities as low as 70 MBq with a maximum absolute difference of 1.3pp.

Since ^{90}Y is a high-energy beta-emitting radioisotope, it raises concerns with regard to the safety of using it for the pretreatment procedure. Low concentrated activity in abdominal organs, such as the stomach, duodenum, and pancreas, may result in a high absorbed dose with dismal consequences. Because of the low incidence of extrahepatic deposition of activity, no dose-effect relationships have been established, but the general consensus is that absorbed doses in abdominal organs are safe up to approximately 50 Gy.[28] Based on the empirically proven safety of a ^{166}Ho pretreatment procedure using 250 MBq, and the fact that ^{90}Y has a 3.11 times higher energy deposition compared to ^{166}Ho, theoretically, a lower activity for the ^{90}Y pretreatment procedure should be used.[8,9,12] That would result in a ^{90}Y activity of around 80–100 MBq, which is above the threshold for accurate LSF estimation using Bremsstrahlung SPECT/CT when reconstructed with an MC-based reconstruction model. The use of 100 MBq of ^{90}Y for the pretreatment procedure could result in a maximum lung dose of 5 Gy (worst case scenario of 100% LSF for 1 kg lungs). This is well below the safety threshold of 30 Gy to the lungs.

On the one hand, low activities for pretreatment procedures are preferred for safety reasons. On the other hand, the activity should also be sufficient to observe any extrahepatic depositions. Prince et al. investigated 34 extrahepatic depositions from a group of 160 patients who received a ^{99m}Tc-MAA injection as part of their radioembolization workup.[9] The extrahepatic depositions had a median activity of 1.3% of the administered activity and a median volume of 6.8 mL. For a ^{90}Y pretreatment procedure using 80 MBq, this would result in an activity concentration of 153 kBq/mL. According to some studies, spheres with low activity concentrations are not visible on PET/CT.[7,14,17] However, these studies were performed to investigate lesion detectability and the spheres in these studies had to be distinguishable from background activity. Extrahepatic depositions are generally located in a cold area, so visibility could be better since there is no background activity. To our knowledge, there are no studies describing the limits of lesion detectability in MC-based reconstruction models for Bremsstrahlung SPECT/CT. However, Dewaraja et al. did describe the visibility of extrahepatic depositions in a ^{90}Y phantom study in which their reconstruction model included MC-based scatter correction.[29] The lowest simulated extrahepatic activity concentration in their study was 108 kBq/mL, and when the MC-based scatter correction was included in the reconstruction model, this extrahepatic deposition was clearly visible. While this result gives confidence in the potential of MC-based Bremstrahlung SPECT/CT for quantification of extrahepatic depositions, the visibility of such depositions with ^{90}Y imaging needs further investigation.

The number of background counts acquired in the PET, SPECT, and planar acquisition protocols were a small

fraction of the total counts for the acquisitions with high activity, but the background counts take up a significant part of the total counts for the acquisitions with low activities (<100 MBq). For these low activities, background correction had a significant impact on LSF estimation.

The SPECT-clinical reconstruction algorithm did not include a background correction. Since SPECT-clinical reconstructions overestimated the LSF for high activities, and a background correction will only impact on low activity scans, this overestimation would probably not be corrected by including a background correction. However, switching to an MC-based reconstruction model, and thereby including scatter correction, does impact the LSF estimation at the full range of activities. Adding an additional background correction to this MC-based reconstruction model again only influences scans with a low activity. Therefore, for Bremsstrahlung SPECT/CT, proper modeling of scatter is more important than including a background correction for accurate LSF estimation. Only for the low activity scans (<100 MBq), a combination of MC-based modeling and background correction is necessary in order to acquire accurate LSF estimations. However, since a background correction seems to underestimate the LSF at low activities (as opposed to a tendency to overestimate the LSF without background correction) one may conservatively choose not to use a background correction.

For the PET acquisitions, the background correction could not be incorporated in the clinical Siemens reconstruction algorithm, like is the case for SPECT-MC-BGcorr, and is therefore performed on an image basis. ^{90}Y PET suffers from low count rate and high random fraction. In addition, there is the natural background signal originating from the ^{176}Lu in the LSO crystal. Both this, and the resulting sparse sinograms, are prone to a positive bias in maximum likelihood reconstructions at low activities.[30] The algorithm used in this study was designed to minimize the effects of algorithm bias to the sparse data. Still, Carlier et al. show that increasing random fractions increase algorithm bias.[15] Their study reports small algorithm bias for random fractions ranging from 0.70 to 0.85. Random fractions in our study ranged from 0.91 to 0.99, indicating we can expect considerably more algorithm bias than observed by Carlier et al. By performing a long background measurement (24 h), we attempted to obtain a reliable background estimation. Subtracting the reconstructed background activity from our reconstructed phantom activity did improve the LSF estimation, but still shows large overestimation of LSF for low activities, indicating that our PET reconstructions suffer more from the algorithm bias than from the background activity. Correcting this algorithm bias requires (partly) redesigning the reconstruction algorithm, which was beyond the scope of this research.

The activity recovery of the PET reconstructions showed good agreement with the study by Willowson et al.[14] They reported good activity recovery for an activity concentration of 37 kBq/mL. We found good activity recovery (less than 10% difference) for activities as low as 45 MBq, which translates to an activity concentration of 41 kBq/mL for the liver compartment and 23 kBq/mL for the lung compartment.

Willowson et al.[31] recommend slightly different reconstruction settings for our scanner (recommended: 2 iterations, 21 subsets; this study: 4 iterations, 21 subsets). For these recommended settings, they show an average error in activity concentration at 300 kBq/mL of −2% (range +4% to −9%). We show an error in activity concentration at 260 kBq/mL of −1%. This error is within the range reported by Willowson et al.

Limitations of our study include that, owing to practical reasons, no phantom data with a 0% LSF were acquired. Therefore, a 0% LSF was simulated by delineating an additional, cold VOI. This simulation of a 0% LSF was suboptimal because the cold VOI was a water compartment instead of a lung-like compartment. Furthermore, the cold VOI compartment in this phantom was located close to the liver. This position resulted in more spillover activity from the liver inside the cold VOI than in the top part of the lung VOI, which is located relatively far from the liver. The effect of the position of the cold VOI in relation to the liver can be observed by comparing the LSF estimations of the planar acquisitions for the 15% and 0% LSF simulations. LSF estimations by planar imaging were heavily influenced by the spillover activity from the liver and resulted in higher LSF estimations for the cold VOI (0%) than for the lung VOI (15%). It is expected that a 0% LSF measurement with no activity in the lungs in a clinical setting would result in less overestimation of the LSF as compared with the current method with the cold VOI.

Another limitation of our study is the fact that MC-based SPECT/CT reconstructions take more time (approximately 3 h) than clinical reconstructions and that MC-based reconstruction algorithms are not available for clinical practice. For availability of the MC-based reconstruction algorithm used in this study, please contact the authors.

Our phantom was filled with ^{90}Y chloride and has uniform activity distribution throughout the liver and the lungs, whereas in a clinical setting, patients treated with ^{90}Y microspheres might have nonuniform activity distribution within the liver and/or lungs. This could influence image quality and quantification and therefore affect LSF estimation.

Another issue that might be encountered in a clinical setting is motion artifacts. Breathing can cause a mismatch between CT and PET or SPECT, which can result in spillover of liver activity into the lungs. This spillover effect can result in an overestimation of the LSF. Yu et al.[4] show that this can be substantially avoided by excluding the region of the lungs that is within 2 cm of the diaphragm.

This study focused on the LSF estimation part of the ^{90}Y pretreatment procedure. It should be regarded as a first step toward application of a ^{90}Y pretreatment procedure. A next step toward implementation could be a multicenter phantom study to verify repeatability, or a clinical patient study including a ^{90}Y pretreatment procedure in combination with a ^{99m}Tc-MAA pretreatment procedure for comparison. This

would require the ordering of a small dosage of ^{90}Y, but it is not uncommon to order multiple vials (one of which could be used for the pretreatment procedure) summing to an overall desired activity, as was done in same-day radioembolization procedures.[32]

5. CONCLUSIONS

This study evaluated the ability to accurately estimate the LSF of ^{90}Y-based radioembolization by means of a low activity ^{90}Y-based pretreatment procedure. The imaging methods investigated comprised PET/CT, Bremsstrahlung SPECT/CT, and planar imaging. Bremsstrahlung SPECT/CT reconstructed with an MC-based model including a background correction can accurately estimate the LSF for a ^{90}Y pretreatment procedure using a theoretically safe ^{90}Y activity as low as 70 MBq.

ACKNOWLEDGMENTS

This project has received funding from the European Research Council (ERC) under the European Union's Horizon 2020 research and innovation program (grant agreement No. 646734).

CONFLICTS OF INTEREST

Marnix G.E.H. Lam is consultant for BTG and Terumo. The department of Radiology and Nuclear Medicine of the UMC Utrecht receives royalties and research support from Quirem Medical/Terumo.

[a)]Author to whom correspondence should be addressed. Electronic mail: b.kunnen@umcutrecht.nl; Telephone: +31 88 7567571; Fax: +31 88 7555491.

REFERENCES

1. Braat AJAT, Smits MLJ, Braat MNGJA, et al. ^{90}Y hepatic radioembolization: an update on current practice and recent developments. *J Nucl Med*. 2015;56:1079–1087.
2. Smits MLJ, Elschot M, Sze DY, et al. Radioembolization dosimetry: the road ahead. *Cardiovasc Intervent Radiol*. 2015;38:261–269.
3. Elschot M, Nijsen JFW, Lam MGEH, et al. 99mTc-MAA overestimates the absorbed dose to the lungs in radioembolization: a quantitative evaluation in patients treated with ^{166}Ho-microspheres. *Eur J Nucl Med Mol Imaging*. 2014;41:1965–1975.
4. Yu N, Srinivas SM, Difilippo FP, et al. Lung dose calculation with SPECT/CT for 90yittrium radioembolization of liver cancer. *Int J Radiat Oncol Biol Phys*. 2013;85:834–839.
5. Lambert B, Mertens J, Sturm EJ, Stienaers S, Defreyne L, D'Asseler Y. 99mTc-labelled macroaggregated albumin (MAA) scintigraphy for planning treatment with 90Y microspheres. *Eur J Nucl Med Mol Imaging*. 2010;37:2328–2333.
6. Hung JC, Redfern MG, Mahoney DW, Thorson LM, Wiseman GA. Evaluation of macroaggregated albumin particle sizes for use in pulmonary shunt patient studies. *J Am Pharm Assoc*. 2000;40:46–51.
7. Khazaee M, Kamali-Asl A, Geramifar P, Rahmim A. Low-dose 90Y PET/CT imaging optimized for lesion detectability and quantitative accuracy: a phantom study to assess the feasibility of pretherapy imaging to plan the therapeutic dose. *Nucl Med Commun*. 2017;1:985–997.
8. Braat AJAT, Prince JF, van Rooij R, Bruijnen RCG, van den Bosch MAAJ, Lam MGEH. Safety analysis of holmium-166 microsphere scout dose imaging during radioembolisation work-up: a cohort study. *Eur Radiol*. 2017; 3:920–928.
9. Prince JF, van Rooij R, Bol GH, de Jong HW, van den Bosch MA, Lam MG. Safety of a scout dose preceding hepatic radioembolization with 166Ho microspheres. *J Nucl Med*. 2015;56:817–823.
10. Smits MLJ, Nijsen JFW, van den Bosch MAAJ, et al. Holmium-166 radioembolisation in patients with unresectable, chemorefractory liver metastases (HEPAR trial): a phase 1, dose-escalation study. *Lancet Oncol*. 2012;13:1025–1034.
11. Prince JF, van den Bosch MAAJ, Nijsen JFW, et al. Efficacy of radioembolization with holmium-166 microspheres in salvage patients with liver metastases: a phase 2 study. *J Nucl Med*. 2017; 4:582–588.
12. Gulec SA, Mesoloras G, Stabin M. Dosimetric techniques in 90Y-microsphere therapy of liver cancer: the MIRD equations for dose calculations. *J Nucl Med*. 2006;47:1209–1211.
13. Selwyn RG, Nickles RJ, Thomadsen BR, DeWerd LA, Micka JA. A new internal pair production branching ratio of 90Y: the development of a non-destructive assay for 90Y and 90Sr. *Appl Radiat Isot*. 2007;65:318–327.
14. Willowson K, Forwood N, Jakoby BW, Smith AM, Bailey DL. Quantitative (90)Y image reconstruction in PET. *Med Phys*. 2012;2012:7153–7159.
15. Carlier T, Willowson KP, Fourkal E, Bailey DL, Doss M, Conti M. (90) Y -PET imaging: exploring limitations and accuracy under conditions of low counts and high random fraction. *Med Phys*. 2015;42:4295.
16. Attarwala AA, Molina-Duran F, Büsing K-A, et al. Quantitative and qualitative assessment of Yttrium-90 PET/CT imaging. *PLoS ONE*. 2014;9:e110401.
17. Carlier T, Eugène T, Bodet-Milin C, et al. Assessment of acquisition protocols for routine imaging of Y-90 using PET/CT. *EJNMMI Res*. 2013;3:11.
18. Pasciak AS, Bourgeois AC, McKinney JM, et al. Radioembolization and the dynamic role of 90Y PET/CT. *Front Oncol*. 2014;4:1–12.
19. Park M-A, Mahmood A, Zimmerman RE, Limpa-Amara N, Makrigiorgos GM, Moore SC. Adsorption of metallic radionuclides on plastic phantom walls. *Med Phys*. 2008;35:1606–1610.
20. van den Hoven AF, Rosenbaum CENM, Elias SG, et al. Insights into the dose–response relationship of radioembolization with resin 90Y-microspheres: a prospective cohort study in patients with colorectal cancer liver metastases. *J Nucl Med*. 2016;57:1014–1019.
21. Floridi C, Pesapane F, Angileri SA, et al. Yttrium-90 radioembolization treatment for unresectable hepatocellular carcinoma: a single-centre prognostic factors analysis. *Med Oncol*. 2017;34:1–12.
22. Sirtex Medical. *SIR-Spheres Yttrium-90 Microspheres Package Insert (CR2014)*; 2016. https://www.sirtex.com/eu/clinicians/package-insert/
23. BTG. *TheraSphere™ Yttrium-90 Glass Microspheres - Instructions for Use*; 2015.
24. Elschot M, Vermolen BJ, Lam MGEH, de Keizer B, van den Bosch MAAJ, de Jong HWAM. Quantitative comparison of PET and Bremsstrahlung SPECT for imaging the in vivo yttrium-90 microsphere distribution after liver radioembolization. *PLoS ONE*. 2013;8:e55742.
25. Elschot M, Nijsen JFW, Dam AJ, de Jong HWAM. Quantitative evaluation of scintillation camera imaging characteristics of isotopes used in liver radioembolization. *PLoS ONE*. 2011;6:e26174.
26. Elschot M, Smits MLJ, Nijsen JFW, et al. Quantitative Monte Carlo-based 90Y SPECT reconstruction. *J Nucl Med*. 2013;54:1557–1563.
27. Klein S, Staring M, Murphy K, Viergever MA, Pluim JP. elastix: a toolbox for intensity-based medical image registration. *IEEE Trans Med Imaging*. 2010;29:196–205.
28. Kao YH, Steinberg JD, Tay YS, et al. Post-radioembolization yttrium-90 PET/CT-part 2: dose-response and tumor predictive dosimetry for resin microspheres. *EJNMMI Res*. 2013;3:1–27.
29. Dewaraja YK, Chun SY, Srinivasa RN, et al. Improved quantitative 90Y bremsstrahlung SPECT/CT reconstruction with Monte Carlo scatter modeling. *Med Phys*. 2017;44:6364–6376.
30. Van Slambrouck K, Stute S, Comtat C, et al. Bias reduction for low-statistics PET: maximum likelihood reconstruction with a modified poisson distribution. *IEEE Trans Med Imaging*. 2015;34:126–136.

31. Willowson KP, Tapner M, Team QUEST Investigator, Bailey DL. A multicentre comparison of quantitative (90)Y PET/CT for dosimetric purposes after radioembolization with resin microspheres: the QUEST phantom study. *Eur J Nucl Med Mol Imaging*. 2015;42:1202–1222.

32. Gabr A, Kallini JR, Gates VL, et al. Same-day 90Y radioembolization: implementing a new treatment paradigm. *Eur J Nucl Med Mol Imaging*. 2016;43:2353–2359.